International Journal of Wavelets, Multiresolution
and Information Processing
Vol. 9, No. 3 (2011) 361–374

DOI: 10.1142/S0219691311004109

WAVELET ANALYSIS FOR STATOR FAULT DETECTION IN INDUCTION MACHINES

SANTIAGO J. GIACCONE, GUILLERMO R. BOSSIO*
and GUILLERMO O. GARCÍA

Grupo de Electrónica Aplicada
Universidad Nacional de Río Cuarto
Ruta Nacional 36 Km 601, C.P. X5804BYA
Río Cuarto, Argentina
**gbossio@ing.unrc.edu.ar*

JORGE A. SOLSONA

Instituto "Alfredo Desages", DIEC
Universidad Nacional del Sur
(*B8000CPB*) *Bahía Blanca, Argentina*
jsolsona@uns.edu.ar

Received 25 June 2009
Revised 7 January 2011

The main objective of the proposed analysis is the detection of inter-turn short circuits in the stator windings of an induction machine. The analysis of the space vector current modulus of an induction motor is presented in this paper. This analysis is based on Daubechies 8 wavelet with seven decomposition levels. The 5th decomposition-level detail signal for a 4 kHz sampling frequency is chosen as a fault indicator, based on simulation results that show different behaviors of the energy contained in the detail signals independent of the percentage of load and fault levels. Experimental results that validate the proposed strategy are also presented. These results also show that the strategy is in addition immune to load variations as well as to feeding voltage unbalances.

Keywords: Wavelet analysis; fault detection; inter-turn short circuits.

AMS Subject Classification: 22E46, 53C35, 57S20

1. Introduction

The early fault detection in industrial electric motors became undoubtedly necessary these days. The Motor Current Signature Analysis (MCSA) of the motor currents, based on the Fast Fourier Transform (FFT), has been used in the industry as a standard. This technique allows measuring the motor currents avoiding additional

*Corresponding author.

sensors like accelerometers.[1,2] The use of FFT is recommended only for steady state, since abrupt variations of either load or speed are reflected in the motor currents and their effects are averaged in the FFT computing process, resulting in dispersion within the spectrum. This dispersion phenomenon may hide useful frequencies for fault detection. Wavelet representation is one of the best options to detect faults under variable speed or load conditions, since it allows analyzing signals during a transient. In addition, given that wavelet basis functions are not unique, other basis functions can be used to project the signals and which may provide useful information.

The wavelet transformation has been used in the fault detection mainly:

On the analysis of vibration signals, in order to detect faults in the bearings and gearboxes, the Morlet Complex Wavelet was used. The wavelet base function selection criteria was based on the energy retained in the decomposition coefficients, or in the ratio between energy and the Shannon entropy of the decomposition coefficients.[3–5]

On the detection of broken bars in squirrel cage induction motors. For instance, in Refs. 6 and 7, the authors used the 8th-order Daubechies Wavelet (due to its continuity) and do not specify sampling frequency at all. However the analysis proposed in these two papers uses high number of decomposition levels since broken bars appear mainly at low frequencies.

On the stator winding short-circuit detection, in Ref. 8 the calculation of the PSD (Power Spectrum Density) for each decomposition level of a 7th-level DB10 wavelet transformation is presented. PSD is calculated for each current of a three-phase motor, with a 6-kHz sampling frequency and is used in the detection of motor short-circuits. The detection method is based on the increase of the energy contained in the detail coefficients, especially that of D2 (1,500–750 Hz) and D3 (750–375 Hz) bands.

The present work aims at studying the space vector current modulus (SVCM) through wavelet analysis to detect short-circuits in the stator windings of induction machines (IM). The proposed strategy allows the detection of this faults independently of the motor load condition. That is possible in motors directly connected to the grid, in which speed on the shaft only depends on the mechanical load coupled to them.

This paper is organized as follows: in Sec. 2 wavelet transform and their implementation using digital filters is introduced. Section 3 contains the procedure to obtain the signal under analysis from the motor currents. In Sec. 4, simulation results for a model of an induction motor with stator-winding short-circuits are used as a benchmark for the development of the detection technique proposed. Experimental results that validates the proposed technique are shown in Sec. 5. Finally, conclusions about the usefulness of the strategy are driven in Sec. 6.

2. Filter Characterization

In Ref. 9, Mallat presents an iterative algorithm, based on digital filters, to calculate the wavelet representation for a given signal, by means of characterizing the quadrature filters necessary for the mentioned algorithm, in terms of their frequency. These filters must fulfill definite conditions in order to keep orthonormality of the basis functions. They also define the shape of scale functions (implemented as Low Pass Filters) and the wavelet associated to them (High Pass Filters). These conditions are detailed in Ref. 10.

An 8th-order Daubechies Wavelet with 16-coefficient filters is used in this work. Several wavelet basis can be selected. The filters used in this particular implementation are FIR, since they are the ones that best fit the requirements for further implementations in on-line schemes, similar to the one proposed in Ref. 11.

3. Space Vector Current Modulus

The space vector current can be obtained by transforming the *abc* currents into a *dq* reference frame. Its components are:

$$i_d = \frac{2}{3}i_a - \frac{1}{3}i_b - \frac{1}{3}i_c, \tag{3.1}$$

$$i_q = -\frac{1}{\sqrt{3}}i_b + \frac{1}{\sqrt{3}}i_c. \tag{3.2}$$

A brief description of the use of this signal for different fault conditions in induction motors is presented in Refs. 12 and 13.

If the three *abc* currents do not show either unbalances or harmonics and the transformed currents, i_q and i_d, are graphed as abscissa and ordinate, respectively, then the result is a perfect circumference. When harmonics are present, each one of them produce different characteristic deformations.

The SVCM is calculated using Eq. (3.3) and it is constant for symmetric currents. On the contrary, it shows variations of twice supply frequency for current unbalances.

$$|I| = \sqrt{(i_d)^2 + (i_q)^2}. \tag{3.3}$$

Figure 1 shows the space vector path in the $d-q$ plane and the time evolution of the SVCM for a set of three currents with 20% unbalance on the phase-b direction.

4. Simulation Results

The simulation results were obtained from a model of multiple coupled circuits.[14,15] The model includes stator and rotor discretization effects as well as slots, eccentricity and skewed bars. Due to this, the obtained current spectrums are similar to those obtained experimentally. The inter-turn short circuit is included in the model as in Ref. 16.

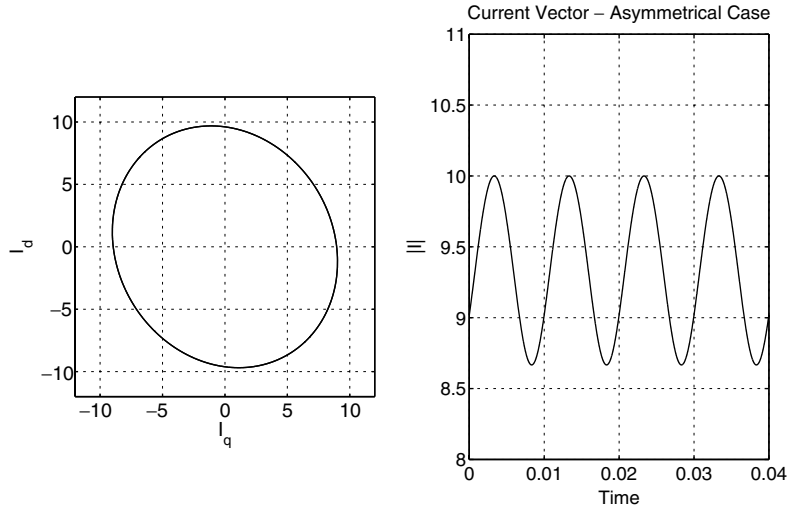

Fig. 1. Current vector trace and time evolution of the SVCM for asymmetric currents with unbalance on phase *b*.

Table 1. Frequencies included in each detail level.

Detail level	Frequency band [Hz]
D1	2,000–1,000
D2	1,000–500
D3	500–250
D4	250–125
D5	125–62.5
D6	62.5–31.25
D7	31.25–16.625
A7	16.625–0

The simulation was carried out using a 4-kHz sampling frequency. The same sampling frequency was used in the experiments.

In this way, the range of frequencies for each decomposition level are presented in Table 1.

The behavior of a motor, loaded every 2 seconds with 0%, 25%, 50%, 75% and 100% rated torque. From this simulation, the SVCM is obtained (Eqs. (3.1)–(3.3)).

Load variations can be observed as DC component step changes in the signal in Figs. 2 and 3. The SVCM for a healthy motor is shown in Fig. 2. The SVCM for similar load conditions and 10 short-circuited turns can be seen in Fig. 3.

Figure 3 also shows an AC component superimposed to the DC component, which indicates the presence of the fault in the motor.

The signals shown in Figs. 2 and 3 are decomposed using a 8th-order Daubechies Wavelet with 7 decomposition levels. The decomposition results can be observed in Figs. 4 and 5, respectively.

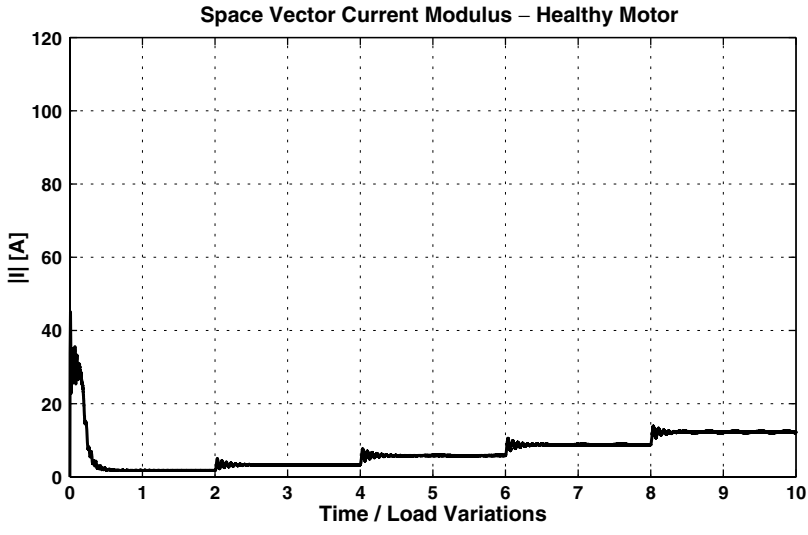

Fig. 2. Time evolution of the SVCM for load variations in a healthy motor.

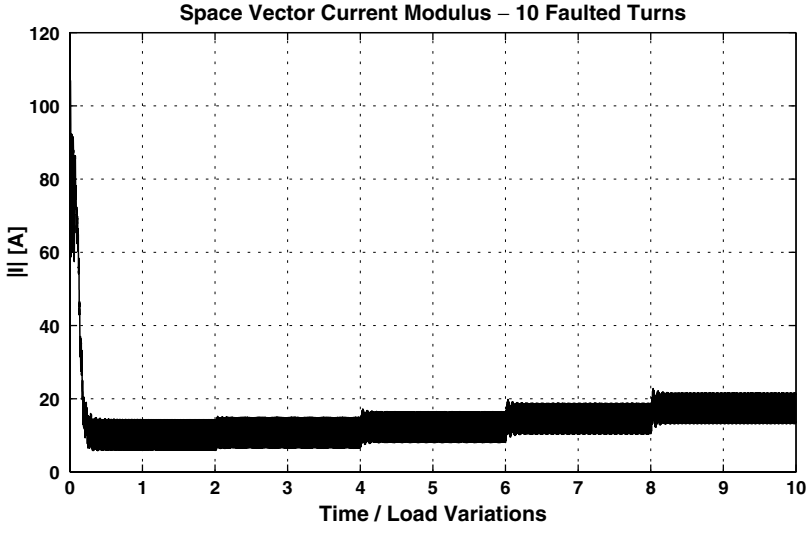

Fig. 3. Time evolution of the SVCM for load variations in a motor with 10 of 144 turns short-circuited.

Due to the characteristics of the signal, load variations are only reflected in the approximation signal **A7** without modifying the signal details.

It can be seen from Figs. 4 and 5 that all the levels of signal details change with the fault magnitude. In order to characterize these decomposition changes due to variations in the number of short-circuited turns, the energy contained in each decomposition level is used.

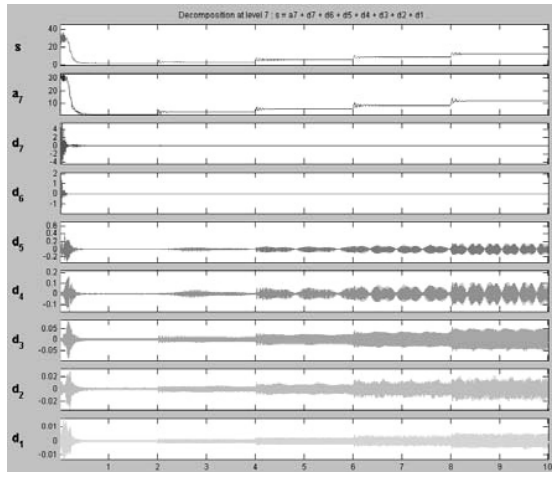

Fig. 4. Load variations for a healthy motor (simulation).

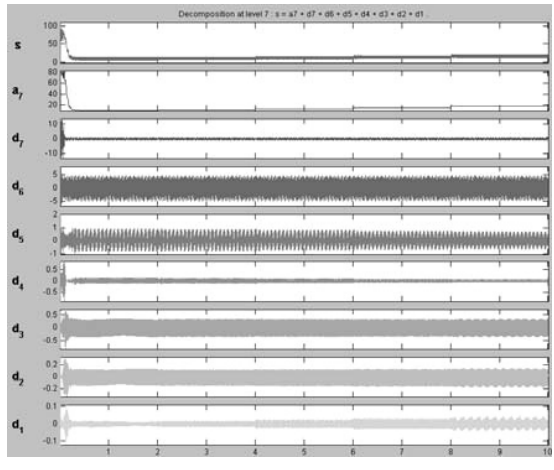

Fig. 5. Load variations for the motor with 10 short-circuited turns (simulation).

By considering a 1 second interval after 7 seconds (Figs. 4 and 5) of running simulation, the energy contained in the signal detail is calculated.

Using Eq. (4.1) the energy percentage contained in each detail level, with $k = 1, \ldots, 7$, is obtained.

$$E_{d_k} = 100 \frac{\sum C_{d_k}^2}{E_t} \tag{4.1}$$

where E_t is the total energy contained in the signal, C_{d_k} the detail coefficients, and C is the sampled signal amplitude

$$E_t = \sum (C^2). \tag{4.2}$$

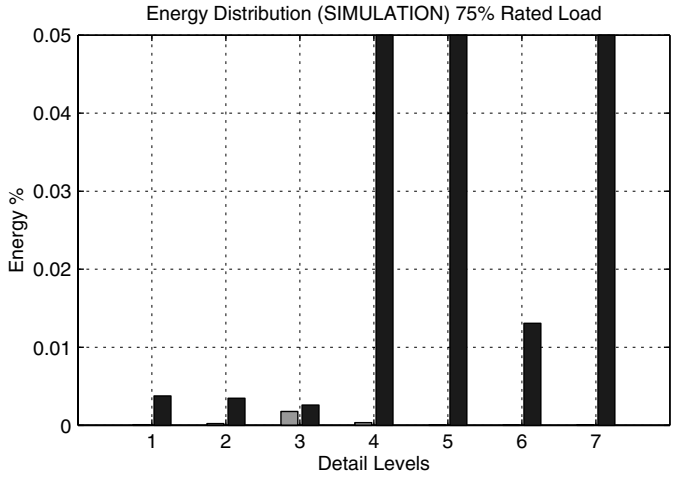

Fig. 6. Energy percentage contained in the coefficient of the decomposition details shown in gray for a healthy motor and in black for a motor with 10 short-circuited turns (simulation).

Since the load condition is the same for both simulations (75%) changes in the signal are only due to the short-circuit fault. These results can be seen in Fig. 6. The energy for a healthy motor is shown in gray bars (left ones) whereas that for a motor with 10 faulted turns, in black bars (right ones). These bar graphics also show how short-circuit disperses the signal energy to all details levels, particularly between **D4** and **D7**.

From the MCSA, it is known that for stator short-circuits, the characteristic frequency is 50 Hz at negative sequence and the SVCM appears as a component at twice the supply frequency (100 Hz).[12] This 100 Hz component is within the **D5** range for the sampling frequency used in this work. The effects of voltage unbalances, which may hide short-circuit effects on the stator currents, are also included in this frequency range.

In addition, it is known that no new harmonic components of the stator currents appear due to inter-turn short circuit. On the contrary, already present frequencies increase, for instance, those of the rotor bars and those near 900–1,300 Hz.[16] The increase in these frequency components must appear as an increase of the energy level **D1** and **D2** in the proposed decomposition. These two levels react to the presence of the fault, but other levels are more sensitive such as **D4**–**D7**.

Figures 7–10 shows the behavior of the energy for every detail level and the approximation energy of decomposition fault signals for 0, 1, 2, 5, and 10 short-circuited turns and for different load values. Particularly, in Fig. 10 can be seen that for the healthy motor, the energy of **A7** is of 100% for the entire load range. If the percentage of faulted turns is increased, energy retained in **A7** decreases compared with the healthy case. This effect is more pronounced for low load conditions.

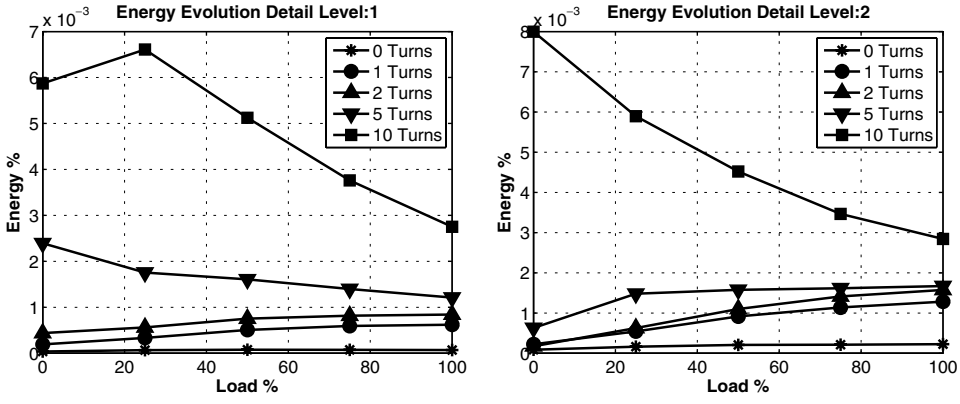

(a) D1 (b) D2

Fig. 7. Energy evolution associated to D1 and D2.

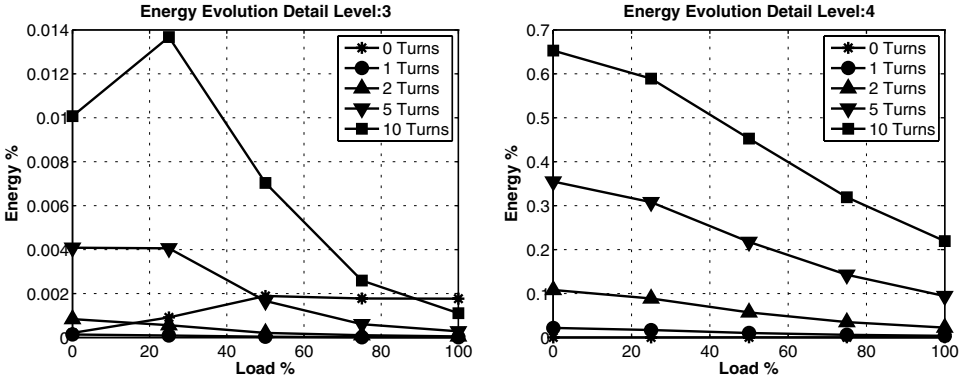

(a) D3 (b) D4

Fig. 8. Energy evolution associated to D3 and D4.

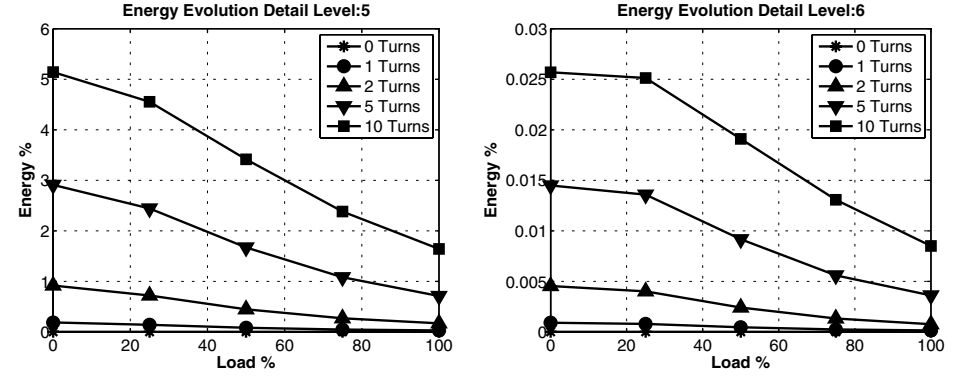

(a) D5 (b) D6

Fig. 9. Energy evolution associated to D5 and D6.

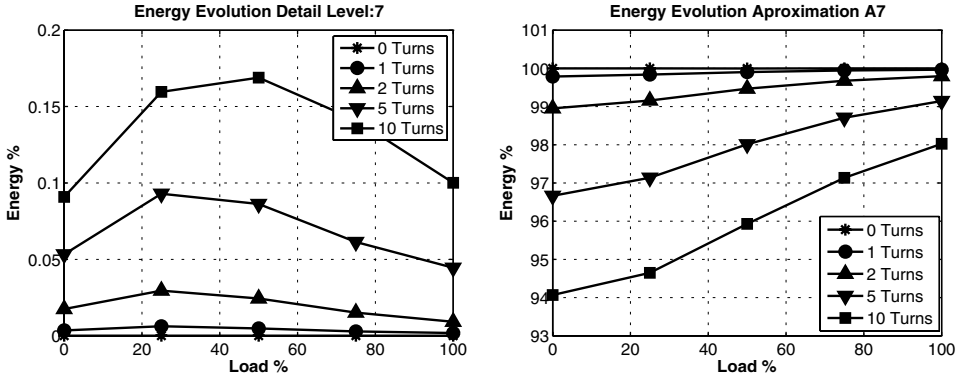

(a) D7 (b) D8

Fig. 10. Energy evolution associated to D7 and A7.

The energy not retained in **A7** scatters to **D1** to **D7**, shown in Figs. 7–10(a).

Level detail **D5** of the proposed decomposition is chosen as short-circuit indicator because its magnitude and its response to the different levels of short-circuit severity.

5. Experimental Results

In order to validate the strategy proposed in the previous section, experimental tests were performed. The experimental setup is shown in Fig. 11. A specially rewounded motor was supplied with the grid 380-V voltage. The characteristics of the motor are presented in Table 2.

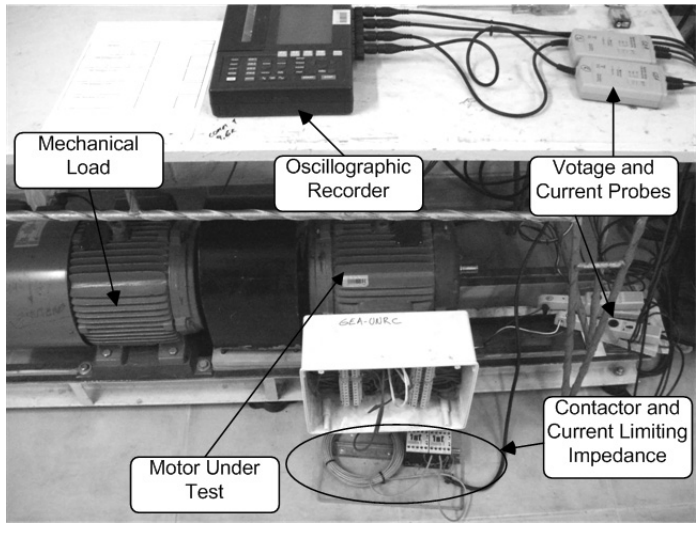

Fig. 11. Experimental setup.

Table 2. Induction motor data.

Power	5.5 kW	Poles	4
Line voltage	380 V	Rated current	11 A
Rated freq.	50 Hz	turns/phase	144

By means of a contactor, a sudden short-circuit is emulated affecting three turns of the stator phase *a*. Since the current in the short circuit has a dangerously high value, an external impedance limiting the fault current was used. The motor under test was loaded by using an IM Drive working as a programmable load.

5.1. *Balanced voltage*

Figure 12 shows the SCVM transient for the motor with balanced feeding voltage and no load 12(a), full load 12(b). The inter-turn short circuit is produced at 1.5 seconds. The effect of the fault is an increase in the signal amplitude for no load and a DC component increase when the motor is working at full load.

In order to verify which of the detail levels is more sensitive to a fault, the energy contained in each decomposition level is again calculated. A portion of the signal trace before the short-circuit (from 0 to 1 seconds) and another after it (from 3 to 4 seconds) are considered for this analysis (Fig. 12). The energy contained in the details levels for this experiment can be clearly observed in Fig. 13.

By comparing Figs. 13(a) and 13(b), the energy contained in 13(b) is lower than that in 13(a) since the energy retained in the approximation is higher than that in the details due to the DC value increased in the signal. In addition, an increase in the **D5** band when a fault occurs can also be observed.

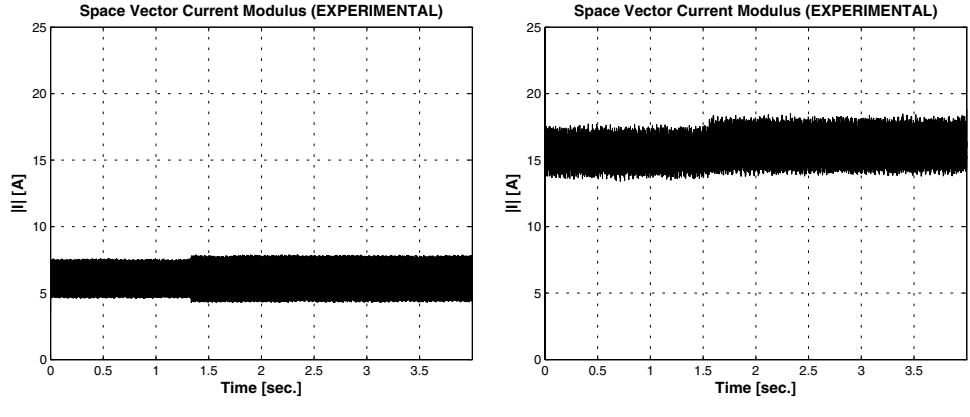

(a) (b)

Fig. 12. SVCM for motor with balanced voltage supply for (a) No load; (b) Full load.

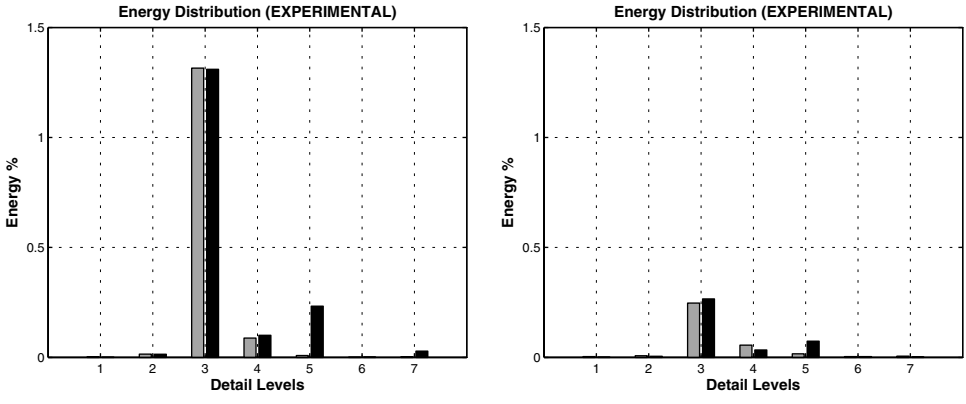

(a) (b)

Fig. 13. Energy of the decomposition details before fault (gray) and after fault (black) with balanced voltage supply for (a) No load; (b) Full load.

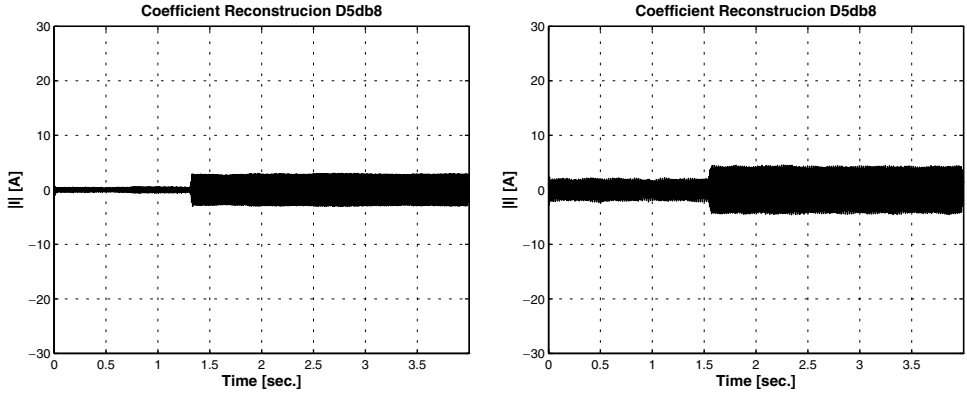

(a) (b)

Fig. 14. Temporal evolution of the D5 coefficients for balanced voltage and (a) No load; (b) Full load.

This increase is reflected in the shape of the **D5** coefficient reconstruction shown in Fig. 14.

5.2. *Unbalanced voltage*

Tests that considers 2.5% voltage unbalance was included to observe the decomposition behavior.

Figures 15–17 shows the test results obtained for a feeding voltage unbalanced of $100(V_{sn}/V_{sp}) = 2.5\%$. By keeping voltage unbalance constant, the motor was tested for no load and for full load.

Figure 15 shows the time evolution of the SVCM.

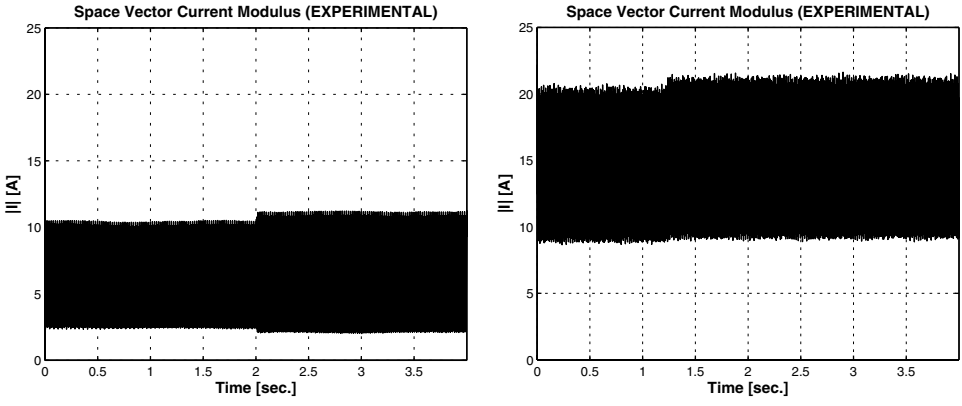

(a) (b)

Fig. 15. SVCM for a motor with 2.5% voltage unbalance and (a) No load; (b) Full load.

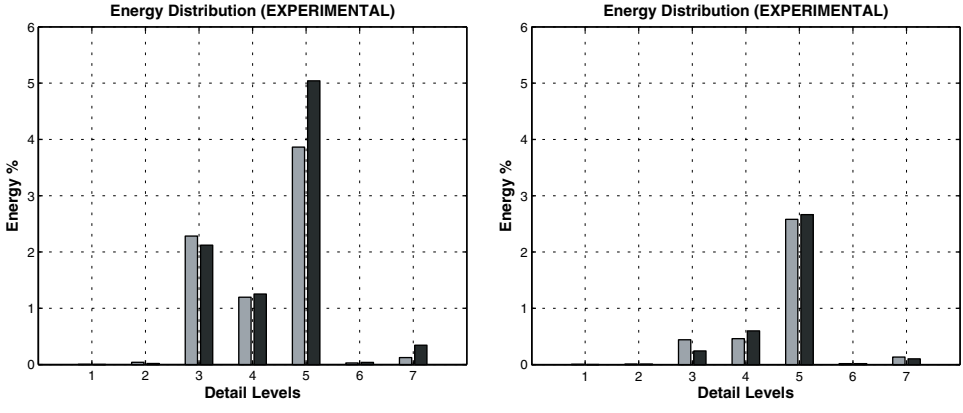

(a) (b)

Fig. 16. Energy of the decomposition details before fault (gray) and after fault (black) for 2.5% voltage unbalance and (a) No load; (b) Full load.

Again, a portion of the signal trace before the short-circuit (from 0 to 1 seconds) and another after it (from 3 to 4 seconds) are considered in order to perform the calculation of the energy content in every detail level. Figure 16 shows a comparison of energy values before and after short-circuit. Finally, Fig. 17 shows the evolution of the reconstruction of the **D5** detail coefficients.

The energy contained in the details is higher for unbalanced than for balanced voltages. **D5** keeps its characteristic of increasing as the motor undergoes fault. However, the increase of energy in presence of a fault on this level is lower than that of the previous case.

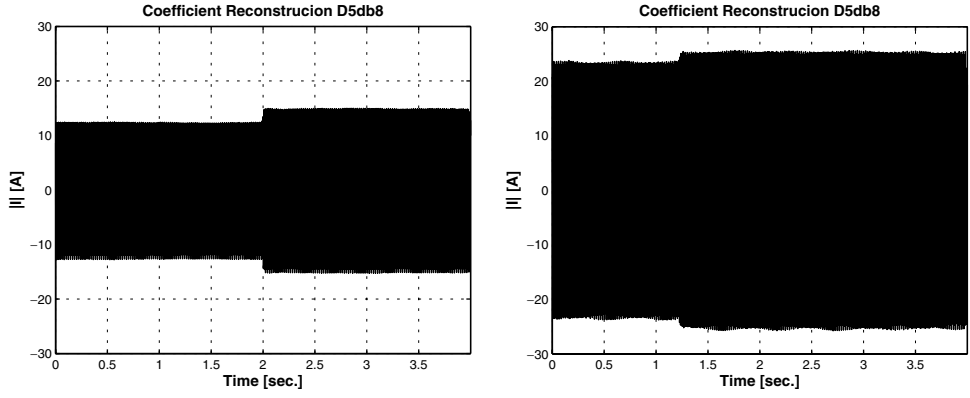

(a) (b)

Fig. 17. Temporal evolution of the D5 coefficients for 2.5% voltage unbalance and (a) No load; (b) Full load.

6. Conclusions

The wavelet analysis of the space vector current modulus (SVCM) presented in this paper allows identifying the presence of inter-turn short circuit. However, it does not allow identifying the faulted winding.

In addition, it is immune to load variations, which is an advantageous characteristic when dealing with the detection of those faults highly dependant on load and the operation frequency.

A 4-kHz sampling frequency was used in this work. The results obtained show an increase of energy at level **D5**. This level includes the 100 Hz component on the SVCM. **D5** also reacts to voltage unbalances, which may mask the presence of stator sort-circuit. However, the energy of this level still increases when a fault occurs, whether for unbalanced supply or in presence of load variations.

Choosing the wavelet decomposition method in this case constitutes an advantage when designing a filter bank for on-line implementations since the filters used for these transformations are well known and their applications widely spread. Allowing the implementation of the first five decomposition levels filters in on-line fault detection implementing only the **D5** level, for a 4 kHz sampling frequency.

The study and characterization of the decomposition response using different basis functions becomes necessary in order to identify the better basis to detect a particular kind of fault. This work is a step in this direction.

Since this is an entirely signal-based analysis, it does not require the motor parameters. Only the motor plate data is needed to use this analysis on field. This simplifies its implementation on industrial predictive maintenance routines.

Acknowledgments

The authors want to thank CONICET, Agencia de Promoción Científica y Tecnológica (ANPCyT), FONCyT, MinCyT, MinCyT-CBA, Universidad Nacional de Río Cuarto and specially to Msc. Lic. Laura Virginia Pérez for their patience and constructive thinking.

References

1. M. F. Cabanas, M. G. Melero, G. Alonso, J. Cano and J. Solares, *Técnicas Para el Mantenimiento y Diagnóstico de Máquinas Eléctricas Rotativas* (Marcombo, 1998).
2. W. T. Thomson and M. Fenger, Current signature analysis to detect induction motor faults, *IEEE Industry Appl. Mag.* **4** (2001) 26–34.
3. Z. K. Zhu, Z. He, A. Wang and S. Wang, Synchronous enhancement of periodic transients on polar diagram for machine fault diagnosis, *Int. J. Wavelets Multiresolut. Inf. Process.* **4** (2009) 427–442.
4. R. Yan and R. X. Gao, Base wavelet selection for bearing vibration signal analysis, *Int. J. Wavelets Multiresolut. Inf. Process.* **4** (2009) 411–426.
5. K. C. Gryllias and I. Antoniadis, A peak energy criterion (p.e.) for the selection of resonance bands in complex shifted morlet wavelet (csmw) based demodulation of defective rolling element bearings vibration response, *Int. J. Wavelets Multiresolut. Inf. Process.* **4** (2009) 387–410.
6. H. Douglas, P. Pillay and A. K. Ziarani, A new algorithm for transient motor current signature analysis using wavelets, *IEEE Trans. Industry Appl.* **5** (2004) 1361–1368.
7. H. Douglas and P. Pillay, The impact of wavelet selection on transient motor current signature analysis, in *IEEE International Conference on Electric Machines and Drives*, San Antonio, Texas, USA (2005), pp. 80–85.
8. J. Cusidó, L. Romeral, J. A. Ortega, J. A. Rosero and A. García Espinosa, Fault detection in induction machines using power spectral density in wavelet decomposition, *IEEE Trans. Industrial Electronics* **2** (2008) 633–643.
9. S. G. Mallat, A theory for multiresolution signal decomposition: The wavelet representation, *IEEE Trans. Pattern Anal. Mach. Intell.* **7** (1989) 674–693.
10. S. G. Mallat, Multiresolution approximations and wavelet orthonormal bases of $L^2(\mathbf{R})$, *Trans. Amer. Math. Soc.* **1** (1989) 69–87.
11. M. Khan, T. S. Radwan and M. A. Rahman, Real-time implementation of wavelet packet transform-based diagnosis and protection of three-phase induction motors, *IEEE Trans. Energy Conversion* **3** (2007) 647–655.
12. S. M. A. Cruz and A. J. M. Cardoso, Stator winding fault diagnosis in three-phase synchronous and asynchronous motors by the extended Park's vector approach, *IEEE Trans. Industry Appl.* **5** (2001) 1227–1233.
13. C. J. Verucchi and G. G. Acosta, Fault detection and diagnosis techniques in induction electrical machines, *IEEE Latin America Trans.* **1** (2007) 41–49.
14. G. Bossio, C. De Angelo, J. Solsona, G. García, and M. I. Valla, A 2-d model of the induction machine: An extension of the modified winding function approach, *IEEE Trans. Energy Conversion* **1** (2004) 144–150.
15. G. R. Bossio, Modelado de las irregularidades del motor de inducción: Aplicaciones en la estimación de posición y el diagnóstico de fallas, PhD thesis, Departamento de Electrotecnia, Universidad Nacional de la Plata Facultad de Ingeniería (2004).
16. G. M. Joksimovic and J. Penman, The detection of inter-turn short circuits in the stator windings of operating motors, *IEEE Trans. Industrial Electronics* **5** (2000) 1078–1084.